Coherent multi-pulsing induced by engineered heterogeneity in diode laser arrays

Greggory Scranton Kendall Golden Olivier Spitz Arindam Mishra Igor Belykh* and Yehuda Braiman**

G. S., O. S., A. M., Y. B
The College of Optics and Photonics (CREOL), University of Central Florida, Orlando, FL 32816, USA
Email Address: olivier.spitz@ucf.edu; yehuda.braiman@ucf.edu
K. G., I. B.
Department of Mathematics and Statistics and Neuroscience Institute, Georgia State University, P.O. Box 4110, Atlanta, Georgia, 30302-410, USA
Email Address: ibelykh@gsu.edu
Y. B
Department of Electrical and Computer Engineering, University of Central Florida, Orlando, FL 32816, USA

Keywords: *Controllable pulsing, Diode laser array, Nonlinear dynamics*

The generation of high-power controlled pulse trains in semiconductor lasers is of significant theoretical and practical interest, with broad applications across many fields. Previous work on diode lasers has primarily focused on single-pulse emission from individual diodes, inherently limiting output power. Here, we demonstrate that large direct-current-driven external-cavity laser arrays, subject only to optical feedback and engineered frequency heterogeneity, can exhibit robust, coherent multi-pulsing dynamics. We uncover a multi-pulse generation mechanism driven by two-cluster formation and heterogeneity-induced interburst oscillations, resulting in desirable features such as multi-GHz operation, high peak power, and nearly perfect phase synchronization. Our results pave the way for designing and manufacturing miniature photonic chip arrays capable of scalable multi-pulse generation. Beyond photonics, the underlying multi-pulse mechanism may be broadly relevant to physical and biological networks, where oscillator heterogeneity can give rise to coherent spiking and bursting dynamics.

1 Introduction

Semiconductor lasers are well known for their excitability under various perturbations that disrupt steady-state operation, with pulsing dynamics playing a crucial role in applications such as optical neurons [1, 2] and photonic processors [3]. Most prior studies have focused on single-laser systems, where controllable pulsing typically requires external mechanisms such as AC driving [4], strong current modulation [5, 6], or unilateral injection [7, 8, 9]. These approaches can generate short pulses, including gain-switched and mode-locked pulses down to picoseconds [10, 11, 12, 13], often aided by saturable absorbers [14]. However, these external methods are difficult to scale, and extending synchronized pulsing to large arrays remains elusive. Numerical studies of arrays with saturable absorbers have demonstrated pulsing, but the pulses tend to propagate spatially rather than synchronize across emitters [15, 16, 17], limiting coherent emission and power scaling [18]. Configurations with two lasers subject to both transverse coupling and optical feedback showed limited success in achieving synchronous pulsing [19, 20], but larger implementations have not exhibited robust collective pulsing [19, 21], and approaches using incoherent feedback [22] remain largely unexplored for scalable array synchronization. Thus, despite advances in pulse generation techniques, achieving robust, synchronized multi-pulse emission across large semiconductor laser arrays without extensive active control remains a critical and open challenge.
Meanwhile, synchronization of oscillatory dynamics in laser arrays has been extensively studied [23, 24, 25, 26, 27, 28, 29, 30, 31, 32, 33, 34, 35, 36, 37], with intrinsic heterogeneity and noise often regarded as disruptive factors. However, since the discovery that disorder can tame spatiotemporal instabilities and induce synchronization in oscillator networks [38, 39], it has been shown, both theoretically and experimentally, that under certain conditions, disorder-induced synchronization and coherent dynamics can emerge across a wide range of physical and engineering systems [40, 41, 42, 43, 44, 45, 46, 47]. Notably, it has been demonstrated that a time-delayed laser array with inherent heterogeneity, composed of broad-area diodes in an external V-shaped cavity, under the right conditions can achieve perfect synchrony [48, 49]. Specifically, while frequency heterogeneity typically degrades phase synchrony, the in-

troduction of misalignment (heterogeneity in time delays) can completely reverse this effect, leading to nearly perfect phase-synchronized behavior [50].

In this work, we address the long-standing challenge of synchronizing single pulsing and, more critically, the inherently difficult multi-pulse dynamics in large semiconductor laser arrays. We demonstrate that large arrays of semiconductor lasers subject to optical feedback and non-local delayed coupling can exhibit robust, high-power, coherent, and periodic pulsing dynamics at multi-GHz frequencies. This coherent pulsing is induced by an engineered frequency-detuning heterogeneity among time-delayed coupled emitters, offering a robust and effective pathway for generating synchronized multi-pulse dynamics. The resulting pulses exhibit narrow widths of tens of picoseconds, tunable intervals between well-separated single and multi-spike trains, and transitions from anti-phase to in-phase locking—key features for coherent beam combining.

Unlike prior studies on single-pulse dynamics, which begin with simplified representations such as the Adler model [51, 52] or the Ginzburg-Landau equations [53], our work is grounded entirely in the realistic and widely used Lang-Kobayashi laser array framework. Despite their significance as theoretical tools for exploring pulsing dynamics, these earlier models lack a direct connection to the physical equations governing semiconductor lasers and were unable to exhibit coherent multi-pulse regimes. Using analytical techniques and numerical simulations, we uncover the underlying mechanism of pulse generation in Lang-Kobayashi laser arrays and demonstrate that certain, possibly broad, distributions of intrinsic laser frequencies lead to the emergence of a two-cluster coherent state that supports both single-pulse and multi-pulse regimes. To accurately predict the parameter space of interest for pulsing within the Lang-Kobayashi model, we further develop a reduced model that reveals an emergent frequency of interburst oscillations and relates it to the number of pulses per unit time, which is close to the cavity round-trip time. This mechanism enables controllable, coherent multi-pulsing dynamics, distinct from the conventional saddle-node bifurcation on an invariant circle (SNIC) that yields only single-pulse solutions [54] observed in the classical time-delayed Adler equation and termed topological solitons [55, 53, 51, 52]. Our findings demonstrate the potential of all-optical pulsing in large laser arrays, offering a scalable route for phase-locked beam combining and enhanced optical power delivery.

2 Results

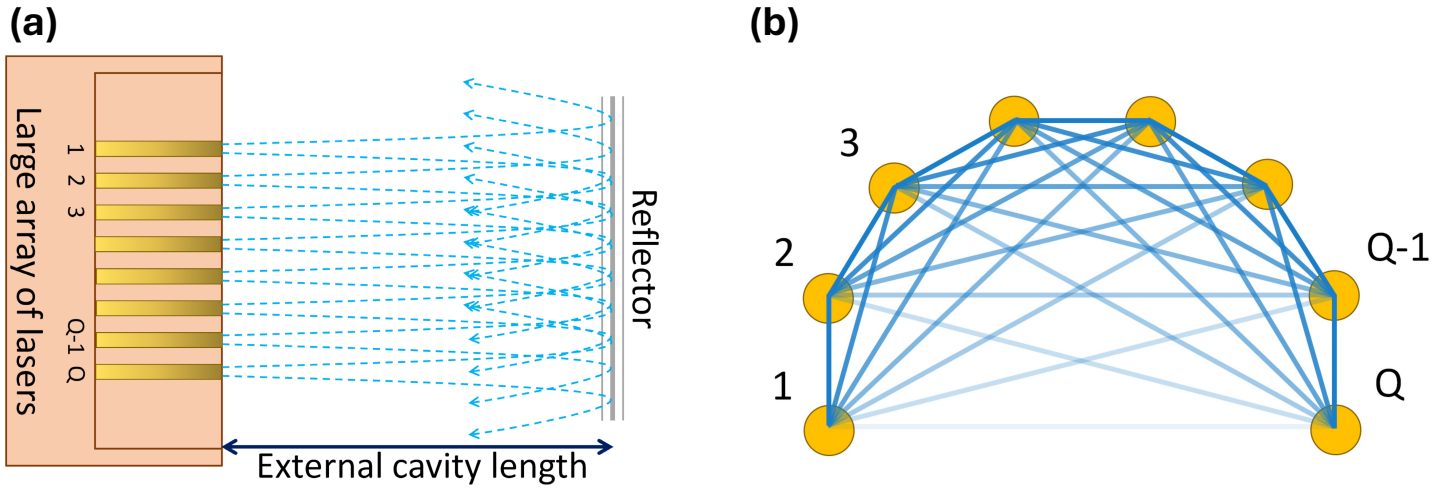

Figure 1: (a) Array of semiconductor lasers subject to decayed non-local coupling and optical feedback. The external reflector provides the feedback and decayed coupling. The reflected beam from each emitter couples to the other lasers in the array after a time delay τ. (b) The equivalent network of emitters with decayed non-local coupling. The transparency of the links is inversely proportional to the coupling strength between emitters. $Q = 30$ for simulations shown in Figs. 2-3.

2.1 Laser array model

We consider a large array of Q delay-coupled semiconductor lasers with decayed non-local coupling described by a version [50] of the Lang-Kobayashi equations [56]:

$$\begin{aligned}\dot{E}_q(t) &= \tfrac{1+i\alpha}{2}\left(g\tfrac{N_q(t)-N_0}{1+s|E_q(t)|^2}-\gamma\right)E_q(t)+i\omega_q E_q(t)+\tfrac{\kappa^f}{Q}\sum_{j=1}^{Q}A_{qj}E_j(t-\tau)\\ \dot{N}_q(t) &= \beta J_{th}-\gamma_n N_q(t)-g\tfrac{N_q(t)-N_0}{1+s|E_q(t)|^2}|E_q(t)|^2,\end{aligned} \tag{1}$$

with the qth laser complex field $E_q(t) = r_q(t)\exp i\phi_q(t)$ and carrier number $N_q(t)$. The parameters are customary for Lang-Kobayashi-type models: g and N_0 are the differential gain coefficient and number of carriers at transparency, respectively, γ is the cavity loss rate, $J_{th} = \gamma_n[N_0 + (\gamma/g)]$ is the pump current threshold, the pump factor $\beta > 1$ means that the lasers are biased above threshold, γ_n is the carrier loss rate, κ^f is the feedback strength. The frequency detuning of the qth laser is ω_q. The time delay τ is the external cavity round-trip time, which is identical for all lasers. $A_{qj} = d^{|q-j|} \in (0, 1)$ is the entry of the decay non-local coupling matrix connecting the qth laser to the jth laser. Although we have computationally verified the emergence of pulses even in the presence of noise and/or non-identical time delays, we have not considered noise and misalignment heterogeneities here in order to explain the pulsing mechanism better and facilitate comparison with the reduced model. Supplementary Table 1 contains the full set of parameter values and their meaning. Figure 1 schematically illustrates the laser array (1). Previous studies within the Lang-Kobayashi framework for a single laser have extensively reported on the dynamical routes to chaos, including stable locking, switching dynamics (particularly in short-cavity regimes [57, 58]) and periodic oscillations [59, 60]. However, these studies have only documented switching dynamics rather than the distinct single-pulse or multi-pulse operation reported in this work (see the Supplementary Material for possible single-laser non-pulsing dynamics). We will also emphasize that pulsing conditions are encountered for moderate-to-strong feedback strengths and bias currents high above the lasing threshold. The latter differs from most of the pulsing schemes mentioned above, which require the laser to be biased close to the threshold to optimize the pulse characteristics.

2.2 Numerical simulations

For a large array of 30 semiconductor lasers, intensity time traces of pulsing are shown in Fig. 2. Several conditions of operation are highlighted to prove the tunability of the pulsing pattern, with a single pulse per period in Fig. 2(b), two pulses per period in Fig. 2(c), three pulses per period in Fig. 2(d), and four pulses per period in Fig. 2(e), with the peculiarity, in the latter, that the time interval between each pulse differs inside a train of pulses. The periodicity of pulses and pulse trains is very close to the external cavity time delay τ. There can be up to three characteristic time scales (one for cavity round-trip time, one for intervals between pulse trains, and one for intervals between the pulses within a single pulse train) at stake in this nonlinear phenomenon. Figure 2 shows two distinct pulsing dynamics within the array, with even-numbered lasers exhibiting one pattern and odd-numbered lasers displaying another pattern. This stems from the choice of frequency detuning set with ω_q in (1) presented in this study ($f_q = \omega_q/2\pi = 2$ GHz for even-numbered lasers and $f_q = -2$ GHz for odd-numbered lasers). This choice of detuning helps illustrate the pulsing mechanism but does not contrast strongly with other detuning configurations detailed in the Supplementary Material. This detuning configuration was engineered to better enable pulsing, although other non-alternating detuning configurations can also induce pulsing. While one might expect the pulse count dependence shown in Fig. 2(a) to exhibit a devil's staircase structure - akin to frequency locking observed in modulated external-cavity semiconductor lasers [61], fiber lasers [62], and frequency comb lasers [63] - the presence of multiple plateaus is more likely a result of multistability among coexisting states in the large, 30-laser array. As we show in the following subsection, the devil's staircase behavior becomes more pronounced in the simpler two-laser configuration.

Figure 3 provides a more detailed view of the overall behavior of the 30-laser array. In the single-pulse case, as shown in Fig. 3(a), the lasers exhibit alternating dynamics: even-numbered lasers follow a sim-

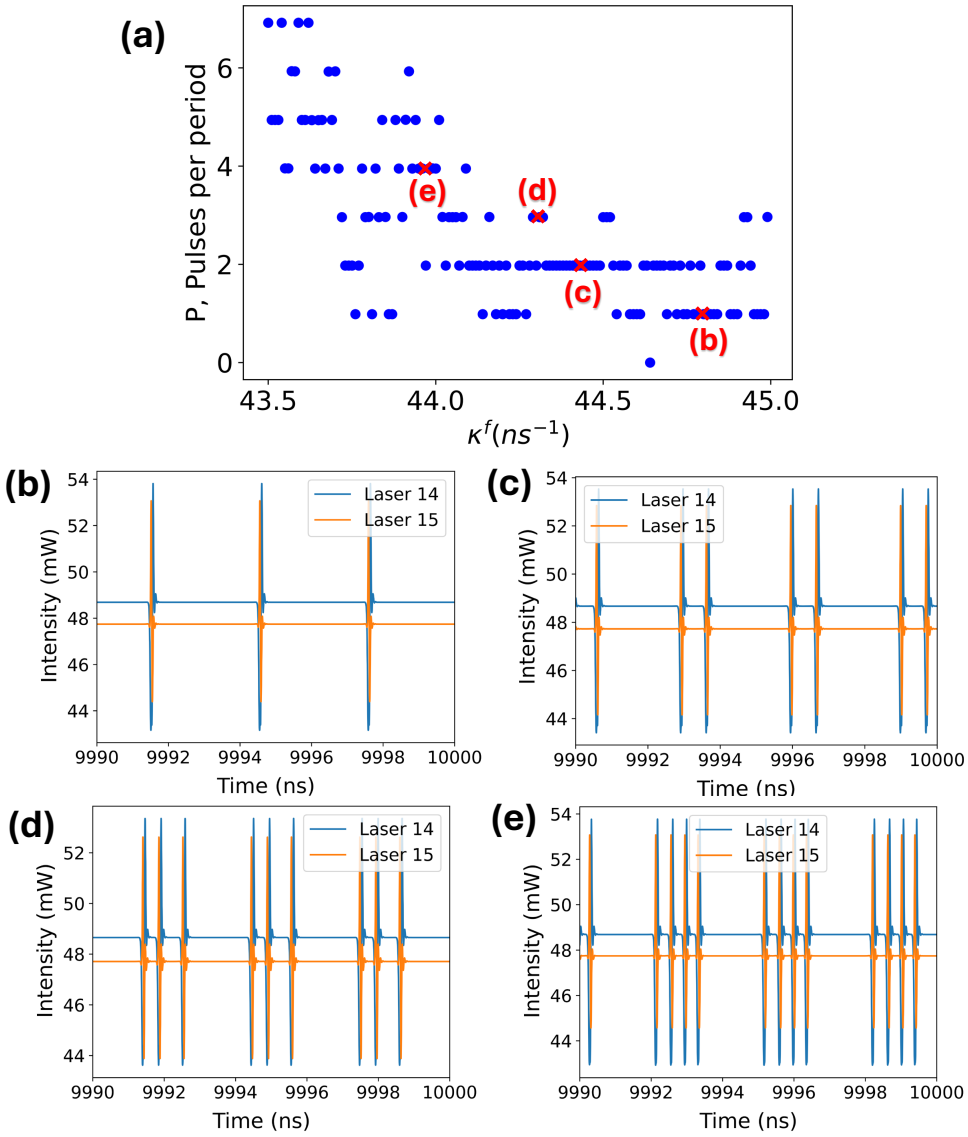

Figure 2: Multi-pulse dynamics in a 30-laser array under varying feedback strength. (a) Number of pulses per period as a function of feedback strength κ^f, obtained from a parameter sweep of the 30-laser system (1) after transient dynamics have been discarded. As κ^f varies, the number of pulses per period switches between discrete values, indicating multistability. The same set of randomly chosen initial conditions is used for all simulations. (b)–(e) Time traces of representative lasers showing distinct pulsing regimes at different values of κ^f: (b) single pulse per period for $\kappa^f = 44.8ns^{-1}$; (c) two pulses per period for $\kappa^f = 44.4ns^{-1}$; (d) three pulses per period for $\kappa^f = 44.31ns^{-1}$; (e) four pulses per period for $\kappa^f = 43.99ns^{-1}$. In each panel (b)-(e), the blue trace corresponds to laser #14, representative of the even-numbered lasers, while the orange trace shows laser #15, representative of the odd-numbered group.

ilar pulsing pattern, while odd-numbered lasers share a distinct yet comparable behavior. The only notable deviation occurs at the edges of the array, where the network interactions are slightly different, resulting in less pronounced pulsing. Figure 3(b) details the evolution of coherence over time, displaying the combined field intensity (black curve) and the Kuramoto order parameter in the inset (blue curve). The combined field intensity is given by: $\mathcal{C}(t) = |\sum_{q=1}^{Q} E_q(t)|^2$. This metric complements the complex Kuramoto order parameter [64, 65], which is defined as $R(t)e^{i\Phi(t)} = \frac{1}{Q}\sum_{q=1}^{Q} \exp(i\phi_q(t))$ and reaches 1 when all lasers are in-phase synchronized and 0 when they are anti-phase synchronized. For comparison, the green curve represents the intensity of one of the even lasers, scaled by 30^2, while the orange curve shows the intensity of one of the odd lasers, similarly scaled. Notably, the bias current used in this configuration - approximately 7 to 9 times above the lasing threshold - places the semiconductor lasers in a regime of highly damped relaxation oscillations [66, 67]. As a result, each emitted pulse is not followed

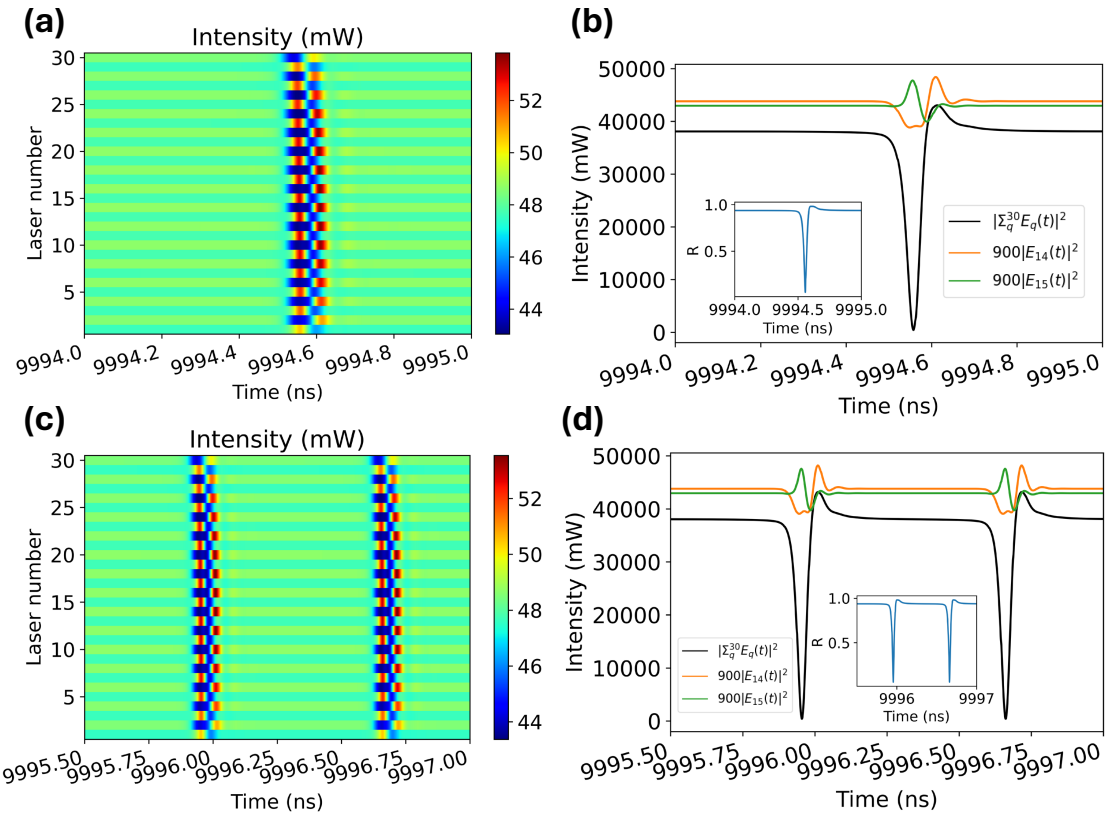

Figure 3: (a) Heatmap of single-pulse dynamics in a 30-laser array with distinct behaviors between odd- and even-numbered lasers. (b) Combined field intensity (black curve) of the 30 lasers, highlighting anti-phase and in-phase synchronization periods. The panel also shows the magnified intensity of an odd laser (green curve) and an even laser (orange curve). The inset demonstrates the Kuramoto order parameter $R(t)$, confirming transitions between anti-phase and in-phase synchrony. The feedback strength $\kappa^f = 44.8ns^{-1}$. (c-d) Same as (a)-(b) but for a pattern with two pulses per period, $\kappa^f = 44.4ns^{-1}$.

by the characteristic ripples typically associated with relaxation oscillations. Another notable feature is the pronounced dip in the combined field intensity, which occurs when the even-numbered lasers pulse. At the dip's lowest point, the lasers are anti-phase synchronized. Within 20 or 30 picoseconds after the Kuramoto order reaches a minimum value, the odd-numbered lasers pulse in phase with the Kuramoto order parameter approaching 1. This alternating pattern between even- and odd-numbered lasers persists when the system is configured for two pulses per period, as seen in Fig. 3(c)-(d), with a strong dip triggered when the even lasers are pulsing. In all other multi-pulsing cases, the pattern remains consistent (not shown). The number of dips in the combined field intensity matches the number of pulses per period, and the Kuramoto order parameter remains high (above 96%) when the odd-numbered lasers are pulsing. Notably, very similar pulsing dynamics are persistent when random perturbations are added to the frequency-detuning values. Supplementary Table 2 gives an example of perturbed detunings that preserve pulsing similar to what is shown in Fig. 3 (see Supplementary Fig. 2). Similar pulse dynamics also robustly appear in a 20-laser array with a sparse frequency detuning configuration (Supplementary Fig. 3). Unlike other laser networks, particularly those using saturable absorbers [15], pulsing in our array occurs simultaneously across all lasers without spatial propagation over time. This results in high-phase synchrony during the pulsing state, which is advantageous for beam combining. Achieving nearly perfect coherence is particularly relevant in large laser arrays, as optical power scales with the square of the number of emitters along the propagation axis.

In realistic laser arrays, the feedback strength may vary across emitters due to angular divergence and wavefront distortions introduced by reflections from the external mirror. While the model (1) already incorporates non-uniform optical feedback through the spatially decaying coupling term A_{qj}, we further investigated the robustness of pulsed dynamics under different types of perturbations, which are detailed

in the Supplementary Material. In particular, we study the impact of the so-called smile effect, most prominently reducing coupling at the array edges [68]. It is relevant to note that in the case of a moderate smile effect, the latter can be corrected with appropriate lensing. Under high-power continuous-wave operation, thermal loading and crosstalk are also unavoidable and may induce slow frequency drifts and spatially varying gain profiles. We thus assessed the impact of these thermal nonuniformities on pulse dynamics and synchronization robustness with two sets of simulations in the Supplementary Material. These results confirm that both slow thermal drift and moderate noise levels do not significantly impair the pulsing dynamics, further reinforcing the robustness of the proposed mechanism. These findings collectively support the robustness of the proposed pulsing mechanism under realistic imperfections, including thermal fluctuations, fabrication-induced asymmetries, and spontaneous emission noise, thereby reinforcing the feasibility of implementing our approach in experimental semiconductor laser arrays.

2.3 Mechanism for pulse generation

To isolate the fundamental mechanisms of pulsing without the complexity of larger arrays, we consider the minimal laser array (1) with $Q = 2$ and $A_{qj} = 1$. This system can be expressed in polar coordinates for the laser field $E_q(t)$ as:

$$\begin{aligned}
\dot{r}_q &= G r_q(t) + \tfrac{\kappa^f}{2} \sum_{j=1}^{2} r_j(t-\tau) \cos\left(\phi_j(t-\tau) - \phi_q(t)\right), \\
\dot{\phi}_q &= \alpha G + \omega_q + \tfrac{\kappa^f}{2} \sum_{j=1}^{2} \tfrac{r_j(t-\tau)}{r_q(t)} \sin\left(\phi_j(t-\tau) - \phi_q(t)\right), \\
\dot{N}_q &= \beta J_{th} - \gamma_n N_q - \left(2G(r_q, N_q) + \gamma\right) r_q^2, \; q = 1, 2,
\end{aligned} \tag{2}$$

where function $G = \frac{1}{2}\left(g\frac{N_q(t)-N_0}{1+sr_q^2(t)} - \gamma\right)$, $r_q(t)$, and $\phi_q(t)$ are the complex field magnitude and phase, respectively. We aim to derive an analytically tractable model that captures how rapid, periodic phase destabilization and pulsing period oscillations, driven by frequency detuning, lead to the emergence of single- and multi-pulse dynamics. Simulations of the array (2), as shown in Supplementary Figs. 10 and 11, suggest two key approximations near the coherent pulsing state: (i) the pulsing period of approximately 8.039 ns is close to the time-delay $\tau = 8$ ns, implying that phase differences $\eta_1(t) = \phi_1(t-\tau) - \phi_1(t)$ and $\eta_2(t) = \phi_1(t-\tau) - \phi_1(t)$ are small; and (ii) $r_1(t)$ and $N_1(t)$ are close to $r_2(t)$ and $N_2(t)$, i.e., $r_1(t-\tau) \approx r_1(t) \approx r_2(t-\tau) \approx r_2(t) \equiv r(t)$ and $N_1(t-\tau) \approx N_1(t) \approx N_2(t-\tau) \approx N_2(t) \equiv N(t)$, where $r(t)$ and $N(t)$ correspond to a nearly coherent state. Further, our simulations indicate that variations in the pulsing periods of both lasers are approximately equal, i.e., we set $\eta_1(t) = \eta_2(t) = \eta(t)$. We then introduce the phase difference $\theta = \phi_1 - \phi_2$ whose evolution is governed by
$\dot{\theta} = \Delta\omega + \frac{\kappa^f}{2}(\sin\left(\phi_2(t-\tau) - \phi_1(t)\right) - \sin\left(\phi_1(t-\tau) - \phi_2(t)\right),$
where $\Delta\omega = \omega_1 - \omega_2$ is a frequency detuning. Similarly, the evolution of r is governed by $\dot{r} = Gr + \frac{\kappa^f}{2} r(t)(\cos\left(\phi_1(t-\tau) - \phi_1(t)\right) + \cos\left(\phi_2(t-\tau) - \phi_1(t)\right)$. Applying the trigonometric identity for the difference of sines, we simplify the θ equation and obtain the reduced system that approximately describes the collective dynamics close to the coherent state:

$$\begin{aligned}
\dot{r} &= Gr + \tfrac{\kappa^f}{2}(\cos\eta(t) + \cos(\theta - \eta(t)))r(t), \\
\dot{\theta} &= \Delta\omega - \kappa^f \cos\eta(t) \sin\theta, \\
\dot{N} &= \beta J_{th} - \gamma N(t) - \left(2G + \gamma\right) r^2.
\end{aligned} \tag{3}$$

Note that the phase difference equation does not contain r and N and represents a variation of the non-autonomous Adler equation [69]. Its behavior is critically governed by the magnitude and evolution of pulsing period variation $\eta(t)$. In what follows, we show how the dynamics of η give rise to generating multi-pulse dynamics.
Supplementary Figure 10 indicates that for single-pulse dynamics, $\eta \approx 0$, allowing us to simplify the θ equation in (3) to the classical non-uniform oscillator form [54]: $\dot{\theta} = \Delta\omega - \kappa^f \sin\theta$. This equation has two fixed points that disappear when $\Delta\omega$ exceeds κ^f. Under the condition that $\Delta\omega$ is slightly greater

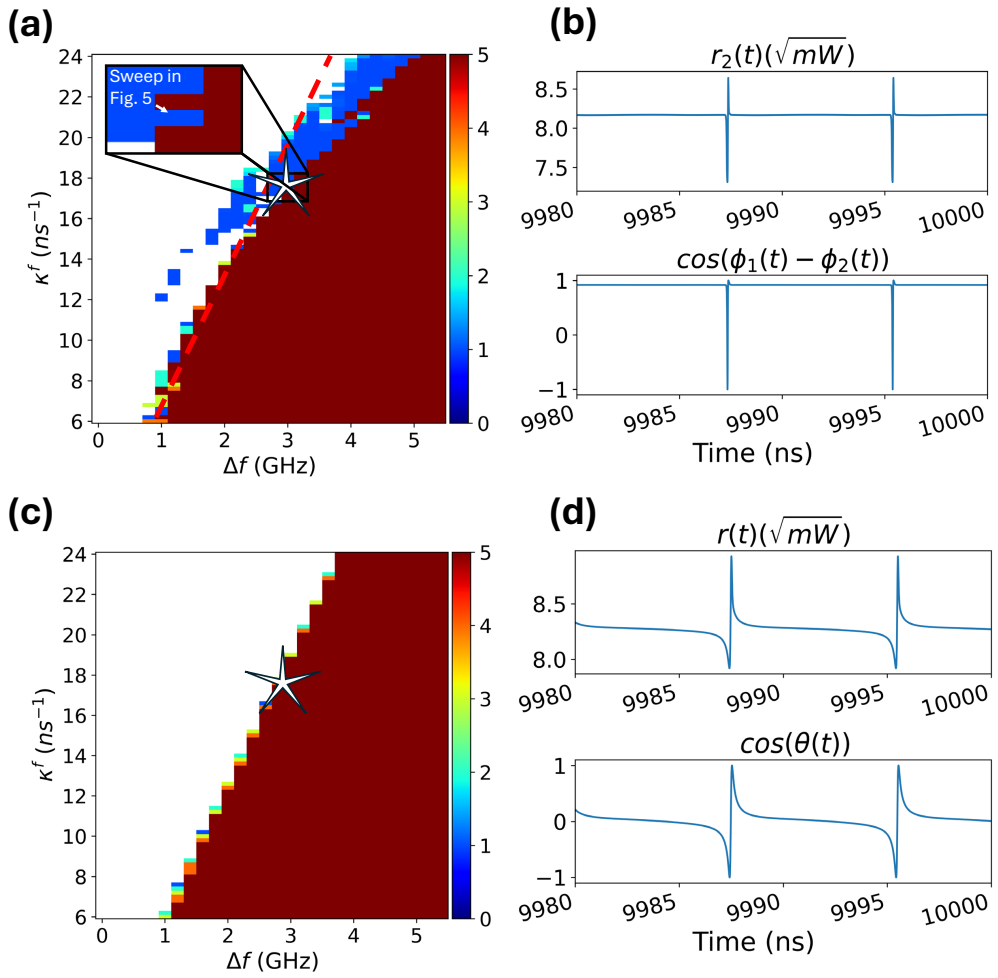

Figure 4: Pulse generation in a two-laser array. (a) Heatmap depicting the number of pulses per round-trip period ($T = \tau = 8$ ns) as a function of the frequency detuning $\Delta f = \Delta\omega/2\pi$ (GHz, x-axis) and the feedback coupling strength κ^f (ns^{-1}, y-axis) in the full Lang-Kobayashi model (2). Each pixel summarizes the outcome of 100 simulations with randomized initial conditions. The color indicates the lowest nonzero number of pulses per period observed, with dark blue representing a single pulse, dark red corresponding to five or more pulses (often associated with fast oscillations), and white indicating steady-state behavior with no pulsing. The inset zooms into the region near the starred parameter set and the arrow marks the direction of the sweep used in Fig. 5. Notably, a gap near $\Delta f \approx 0.9$ GHz marks the minimum detuning required to initiate pulsing. (b) Time trace of $r_2(t)$ for the marked parameter set ($\Delta f = 2.9192$ GHz, $\kappa^f = 17.5808$ ns^{-1}). Although only r_2 is shown, $r_1(t)$ exhibits similar pulse dynamics. (c) Heatmap for the reduced model (3) with $\eta = 0$, plotted over the same parameter range using a single initial condition per pixel. The red dashed curve in (a) indicates the saddle-node bifurcation $\kappa^f = \Delta f$ in the reduced model, accurately predicting the pulsing onset in the full model. (d) Corresponding time trace from the reduced model at the same parameter values. Model parameters for these simulations are listed in Supplementary Table 3.

than κ^f, θ slowly drifts near a ghost state, emerging from a saddle-node bifurcation at $\Delta\omega = k^f$, before rapidly completing the cycle. This rapid increase in the phase difference with θ reaching π destabilizes the r equation via the increased positive term $(1 + \cos\theta)$ and induces a pulse in r. The time between the pulses is determined by the nonuniform oscillator's period [54]: $T_{period} = 2\pi/\sqrt{\Delta\omega^2 - (k^f)^2}$, where the denominator is small. Figure 4 shows that the reduced model (3) with $\eta = 0$ accurately predicts the onset of coherent single-pulse dynamics in the full Lang-Kobayashi model (2), induced by frequency heterogeneity through a saddle-node bifurcation on an invariant circle (SNIC) [54]. This mechanism is consistent with earlier analyses of the autonomous, time-delayed Adler equation and has been linked phenomenologically to pulsing in laser arrays [53, 51, 52]. However, unlike prior work, our derivation explicitly connects this mechanism to the Lang-Kobayashi model via the reduced system (3). It is important to emphasize an essential distinction between the single-pulsing observed in our system and conventional mode-locking [70]. In standard mode-locking, the pulse repetition rate must exactly match

the round-trip time of the external cavity; even slight deviations disrupt phase coherence and break the mode-locking condition. In contrast, the coherent pulsing observed here does not require an exact match between the pulse period and the cavity delay. Although the periods are close, they are not identical. This is clearly demonstrated in Supplementary Fig. 11, where the observed pulse periods are 8.039 ns and 3.037 ns for external cavity delays of 8 ns and 3 ns, respectively. Nevertheless, as with its autonomous Adler counterpart, the simplified, reduced model (3) with $\eta \approx 0$ has a fundamental limitation: it cannot account for multi-pulse dynamics. Capturing such behavior requires retaining the *time-dependent* nature of $\eta(t)$, allowing the pulsing period to oscillate.

From a historical perspective, we first derived the reduced model (3), which suggested that small, persistent oscillations in η could introduce a second emergent frequency governing the number and spacing of multiple pulses per cycle. This theoretical insight was subsequently confirmed through simulations of the full model (2), which revealed the critical role of oscillatory pulsing periods in the emergence of multi-pulse dynamics.

Figure 5 illustrates the emergence of multi-pulse dynamics in the full model (2), focusing on the parameter region highlighted in the inset of Fig. 4. By varying the feedback strength κ^f and the frequency detuning magnitude in a way that keeps the system near the saddle-node bifurcation transition from single- to multi-pulse regimes, we observe a dependence of the pulse number p that resembles a devil's staircase (Fig. 5(a)). Unlike the more fragmented dependence seen in the 30-laser array (Fig. 2), the two-laser system (2) exhibits a classical, well-defined staircase structure. Remarkably, Figs. 5(b)-(d) reveal predicted oscillating behavior in $\eta_2 = \phi_2(t-\tau) - \phi_2(t)$ which governs the number of generated pulses per period. This oscillatory behavior is evident in the periodic repetition of the local maxima of η_2.

Figure 6 presents simulations of the reduced model (3) where $\eta(t)$ is taken from the full model (2). These results confirm that the reduced model successfully captures the emergence and structure of multi-pulse dynamics observed in the full Lang-Kobayashi system (2). Moreover, it sheds light on the underlying mechanism of multi-pulse generation, which rests on two key features: (i) the θ equation of reduced system (3) undergoes a saddle-node bifurcation at fixed values of $\eta^* = \pm\arccos(\Delta\omega/\kappa^f)$; and (ii) the oscillating behavior of $\eta(t)$ enables the phase θ to make multiple 2π rotations during intervals where $|\eta(t)| > |\eta^*|$, i.e., when $\dot{\theta} > 0$. The number of such rotations per cycle determines the number of pulses p. During the remaining portion of the cycle where $|\eta(t)| < |\eta^*|$, the phase θ remains at a stable fixed point corresponding to a quiescent (non-pulsing) phase.

To illustrate the multi-pulse generation mechanism more transparently, we introduce a phenomenological model in the form of a non-autonomous Adler equation [69], which captures the behavior of the reduced model's phase dynamics and simplifies analytical treatment. The model takes the form:

$$\frac{d\theta}{dt} = \Delta\omega - \kappa^f(1 + a\cos\Omega t)\sin\theta, \tag{4}$$

where Ω represents the emerging angular frequency associated with the oscillations in $\eta(t)$ and a is a scaling factor modulating the amplitude of the periodic forcing. The motivation behind the system (4) lies in replacing the periodic term $\cos\eta(t)$ with a periodically modulated expression, $(1 + a\cos(\Omega t))$. This substitution transforms a model that would otherwise support a single-pulse regime into one capable of generating single and multiple pulses per period, with the modulation amplitude a governing the emergence, strength and the shape of the pulsing behavior. As shown in Supplementary Figure 12, the minimum of the potential energy is directly related to the number of pulses in each pulse train. The analysis of this phenomenological model (4), detailed in the Methods section, yields an explicit expression for the number of pulses per modulation cycle as a function of the system parameters:

$$p = F(a, \Omega, \Delta\omega, k^f) \tag{5}$$

with the right-hand side function given via (13)-(14) (see Methods). As shown in Fig. 7, the analytical prediction for p closely matches the results from the direct simulations of the phenomenological model (4), further validating the proposed multi-pulse mechanism.

To further elucidate the mechanism behind the emergence of multi-pulse dynamics, we draw an analogy between the phenomenological model (4) and an overdamped pendulum with a periodically varying

length. Specifically, consider a pendulum of length $l(t) = L + A\cos\Omega t$ subject to a constant torque Γ. In the overdamped regime, where inertial terms are negligible, the equation of motion reduces to

$$\dot{\theta} = \Gamma - L(1 + a_1 \cos\Omega t)\sin\theta, \tag{6}$$

with $a_1 = A/L$. This model is mathematically equivalent to the phenomenological model (4), with the constant torque Γ representing the frequency detuning $\Delta\omega$. In this analogy, the pendulum accumulates potential energy while resting near the bottom of the potential well, and releases it as kinetic energy during rapid rotations, akin to optical pulse emission. As the length $l(t)$ increases, the gravitational restoring force strengthens, deepening the potential well. Conversely, when $l(t)$ decreases, the well flattens, reducing the energy barrier for escape. This modulation of potential depth effectively controls the timing and number of phase slips (rotations) per cycle. As shown in Supplementary Fig. 12, there is a clear correlation between the number of emitted pulses and the depth of the potential energy minima: larger modulation amplitudes a_1 lead to deeper wells, which correspond to greater energy accumulation and subsequently more pulses. These results support the interpretation of multi-pulsing as a mechanism of energy storage and periodic release, regulated by the external modulation. Full derivation and additional illustrations of the pendulum model are provided in the Supplementary Material.

3 Discussion

While single-pulsing in diode lasers is a well-established phenomenon, it typically requires additional mechanisms, such as external current modulation or saturable absorbers, to induce pulsing. In contrast, the multi-pulsing dynamics we uncovered arise naturally from engineered frequency detuning and appropriate selection of diode and external cavity parameters, without any active modulation. Building on this foundation, we addressed a long-standing challenge in photonics, namely the realization of synchronized multi-pulse generation in large semiconductor laser arrays—a key bottleneck in scaling high-power pulsed optical systems. We show that direct-current-driven external-cavity arrays, subject only to optical feedback and non-local time-delayed coupling, can robustly produce periodic, coherent, high-power pulse trains, including complex multi-pulse structures. Rather than relying on external forcing, this behavior arises intrinsically from engineered heterogeneity in intrinsic laser frequencies, offering a powerful, experimentally accessible design principle for achieving scalable, highly controllable multi-pulsing in integrated photonic platforms.

We uncovered the underlying mechanism within the Lang-Kobayashi laser framework, showing that certain, potentially wide, distributions of intrinsic laser frequencies give rise to a two-cluster coherent state that supports both single- and multi-pulse regimes. The onset of multi-pulsing is governed by interburst oscillations induced by frequency heterogeneity. These dynamics are captured by a reduced model explicitly linked to the Lang-Kobayashi equations and further clarified through a phenomenological, analytically tractable version resembling a non-autonomous Adler equation. Together, these models reveal that the number of pulses per burst is accurately determined by the emergent interburst frequency. Importantly, the period of coherent pulsing closely follows the external cavity round-trip time, with subtle, time-varying deviations. These deviations align with the phase difference between the two laser clusters, as supported by Supplementary Fig. 11. This observation underscores the crucial role of frequency heterogeneity, both between and within clusters, in shaping the phase dynamics that ultimately determine the number of pulses in each cycle.

Our analysis assumes identical feedback phases across the array, i.e., no feedback misalignment, enabling the derivation of a consistent analytical framework that bridges the Lang-Kobayashi and Adler models. However, our findings are not limited to this idealized setting. Simulations incorporating delay-time perturbations (e.g., a 20 ps standard deviation) show that coherent pulsing persists even when the feedback phase varies randomly between lasers. This robustness suggests that phase alignment is not a strict requirement for realizing coherent, controllable pulsing in large arrays. Remarkably, we demonstrate that pulse characteristics are strongly dependent on the detuning pattern across the array. This suggests that

coherent pulse generation can be experimentally controlled via methods such as individual bias-current tuning and other means.

The pulsing dynamics reported in this work fundamentally differ from conventional mode-locking, which requires equidistant longitudinal modes with fixed phase relations in a single multimode cavity. In contrast, our system consists of delay-coupled semiconductor lasers with engineered detunings and coupling structure that support robust multi-pulsing even in the presence of phase disorder. Although the lasers become effectively multimode during pulsing, the observed pulses arise not from the standard balance of dispersion and nonlinearity but from the underlying phase-space topology of the coupled system. These localized structures are discrete, robust, and topological, similar in spirit to the dissipative phase solitons described in other nonlinear systems [53].

Very recently, coherent picosecond bright solitons were experimentally demonstrated on a DC-driven mid-infrared quantum cascade laser chip [71]. In that work, laser pulses emerge from a fast bistable nonlinear resonator, eliminating the need for external modulation or saturable absorbers [72] — a significant milestone toward realizing a miniature, integrated photonic chip that emits very narrow, high-frequency pulses. While the specific laser architecture, pulse generation mechanisms, and pulsation patterns may differ—particularly in the recent demonstration, which focuses on single-pulse emission—the generation of narrow, high-frequency, high-power, periodic, and controllable multi-pulse trains in DC-driven external-cavity diode laser arrays in our model also makes it a promising candidate for compact photonic designs targeting diode lasers governed by relaxation oscillation limits. This self-organized, periodic pulse formation arises solely from direct current drive and time-delayed optical feedback, with a notable distinction in our setting: the emergence of coherent multi-pulse dynamics across large laser arrays. These recent experimental advances [71] support the broader relevance of our theoretical findings and underscore the growing convergence between active and passive nonlinear photonic systems.

4 Conclusion

We demonstrated that direct-current-driven external-cavity laser arrays, relying solely on optical feedback and non-local time-delayed coupling, can generate periodic, coherent, high-power, and high-frequency pulses and pulse trains. We have uncovered the pulse generation mechanism originating from a disorder-induced saddle-node bifurcation, which facilitates energy accumulation and subsequently triggers the emission of pulses. Pulse characteristics depend on diode array detuning patterns, allowing pulses to be experimentally realized and controlled by engineering frequency detunings via, for example, individual control of bias currents or other means. Our approach opens new avenues for practical applications, including high-power pulse beam combining and neuromorphic optical computing. Furthermore, the disorder-induced mechanism of coherent pulse generation promises to have substantial implications beyond laser arrays, extending to other excitable physical and biological systems.

5 Method Section

5.1 Analysis of the phenomenological model

The dynamics of the phenomenological model (4) can be analyzed using a slow-fast decomposition. Rewriting the model in rescaled time $t_{new} = \kappa^f t$, we obtain

$$\begin{aligned} \frac{d\theta}{dt_{new}} &= \nu - (1 + a\cos\psi)\sin\theta, \\ \frac{d\psi}{dt_{new}} &= \mu, \end{aligned} \tag{7}$$

where $\nu = \frac{\Delta\omega}{\kappa^f}$, $\frac{\Omega}{\kappa^f} = \mu$, and the auxiliary variable $\psi = \Omega t$ captures the phase of the time-varying modulation. In this formulation, θ is the fast variable, and ψ evolves slowly when $\mu \ll 1$, enabling the use of singular perturbation techniques to analyze the system. We treat ψ as a slowly varying parameter in the fast subsystem, which provides a sequence of phase portraits that govern the overall system dynamics and shape the emergence of multi-pulsing behavior.

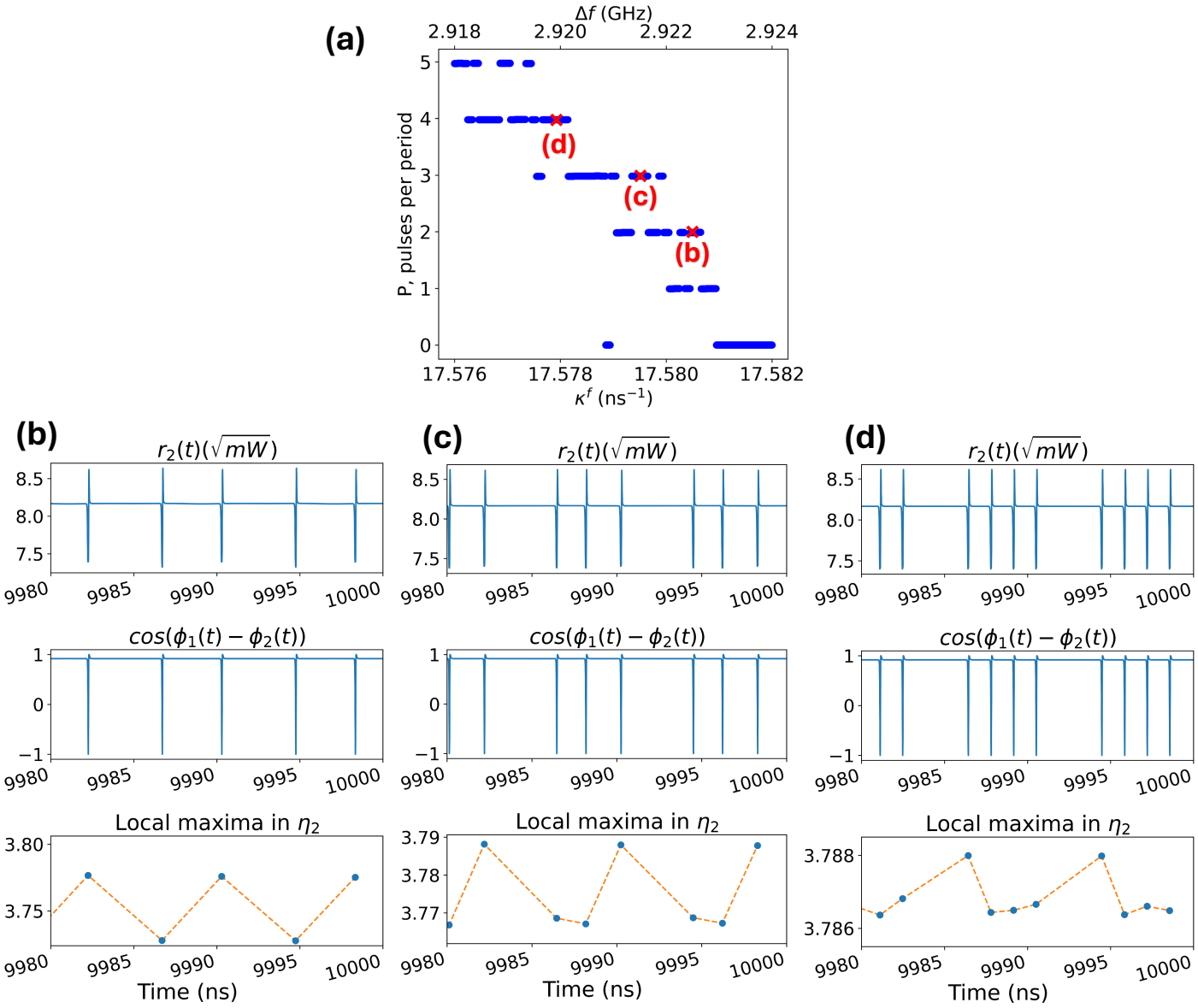

Figure 5: Multi-pulse dynamics in the two-laser model (2). (a) Number of pulses per period obtained from a parameter sweep, where the feedback strength κ^f is increased while the frequency detuning Δf is decreased by the same numerical value, following the dependence shown in the inset in Fig. 4. (b)-(d) Time traces of $r_2(t)$ and $cos(\phi_1(t) - \phi_2(t))$, along with the peak values $\eta_2 = \phi_2(t - \tau) - \phi_2(t)$, for representative cases exhibiting increasing numbers of pulses per period: (b) two pulses per period: $\kappa^f = 17.5805$ ns^{-1} and $\Delta f = 2.9195$ GHz; (c) three pulses per period: $\kappa^f = 17.5795$ ns^{-1} and $\Delta f = 2.9205$ GHz; (d) four pulses per period: $\kappa^f = 17.5779$ ns^{-1} and $\Delta f = 2.9221$ GHz. In all cases, oscillations in η_2 exhibit periodic behavior with a period close to τ. Similar behavior is observed in $\eta_1 = \phi_1(t - \tau) - \phi_1(t)$ [not shown].

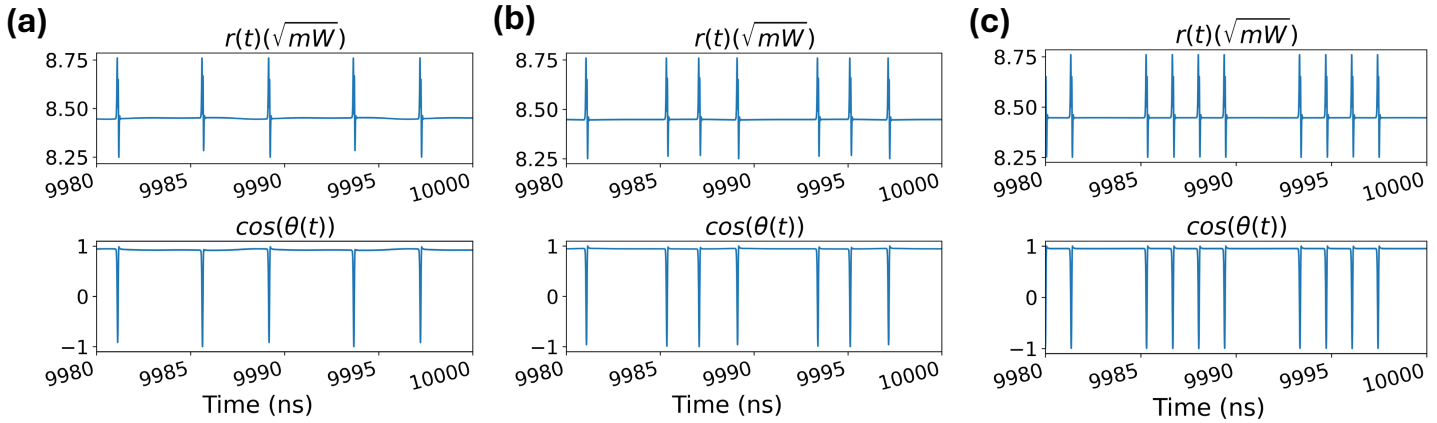

Figure 6: Multi-pulse dynamics in the reduced model. Time traces of $r(t)$ and $\cos\theta$, calculated from the reduced model (3) with time-dependent $\eta(t) \equiv \eta_1 = \phi_1(t-\tau) - \phi_1(t)$, where $\eta(t)$ is taken from the full model. (a)-(c) Simulations correspond to the two-, three-, and four-pulsing regimes observed in Fig. 5(b)-(d), using the same values of κ^f and Δf. (a) Two pulses per period: $\kappa^f = 17.5805$ ns $^{-1}$, $\Delta f = 2.9195$ GHz; (b) three pulses per period: $\kappa^f = 17.5795$ ns $^{-1}$, $\Delta f = 2.9205$ GHz; (c) four pulses per period: $\kappa^f = 17.5779$ ns $^{-1}$, $\Delta f = 2.9221$ GHz. The reduced model predicts the pulsing dynamics of the full system with high accuracy, capturing both pulse multiplicity and timing.

1. Fast subsystem. Setting $\mu = 0$, we obtain the fast system:

$$\begin{aligned} \tfrac{d\theta}{dt_{new}} &= \nu - (1 + a\cos\psi)\sin\theta, \\ \psi &= C, \end{aligned} \tag{8}$$

where C is a constant. This system mimics the reduced model (3) with constant η and, as such, supports only single-pulse generation via a SNIC bifurcation.

Case I. When $\cos\psi < \frac{\nu-1}{a}$, the system (8) has no fixed points and undergoes continuous phase rotation with the period

$$T(\psi) = \frac{2\pi}{\sqrt{\nu^2 - (1 + a\cos\psi)^2}}. \tag{9}$$

The interval of the system's phase rotation is

$$I_{rot} = \{\psi_0 < \psi < 2\pi - \psi_0\}, \quad \text{where} \quad \psi_0 = \arccos\left(\frac{\nu - 1}{a}\right). \tag{10}$$

Case II. When $\cos\psi > \frac{\nu-1}{a}$, the system (8) has a stable fixed point $\theta^* = \arcsin(\frac{\nu}{1+a\cos\psi})$ and phase rotation ceases. The fixed-point regime occurs within the interval $I_{fp} = \{-\psi_0 < \psi < \psi_0\}$.

2. Full system dynamics. For $\mu > 0$, ψ evolves slowly, and the full system (7) alternates between rotational (Case I) and fixed-point (Case II) dynamics. The duration spent in the rotation interval I_{rot} is:

$$T_{rot} = (2\pi - 2\psi_0)/\mu. \tag{11}$$

During this interval, the phase θ can make full 2π rotations. The number of such rotations determines the number of pulses p within the rotation interval I_{rot}. The average period of the rotation time that yields one pulse can be estimated as:

$$T_{pulse} = \frac{1}{2\pi - 2\psi_0} \int_{\psi_0}^{2\pi-\psi_0} T(\psi)\, d\psi, \tag{12}$$

with $T(\psi)$ and ψ_0 are given in (9) and (11), respectively. Therefore, the average number of pulses can be calculated as:

$$p = \frac{T_{rot}}{T_{pulse}} = \frac{(2\pi - 2\psi_0)^2}{\mu \int_{\psi_0}^{2\pi-\psi_0} T(\psi)\, d\psi} = \frac{(2\pi - 2\psi_0)^2}{\mu \int_{\psi_0}^{2\pi-\psi_0} \frac{2\pi}{\sqrt{\nu^2-(1+a\cos\psi)^2}}\, d\psi}, \tag{13}$$

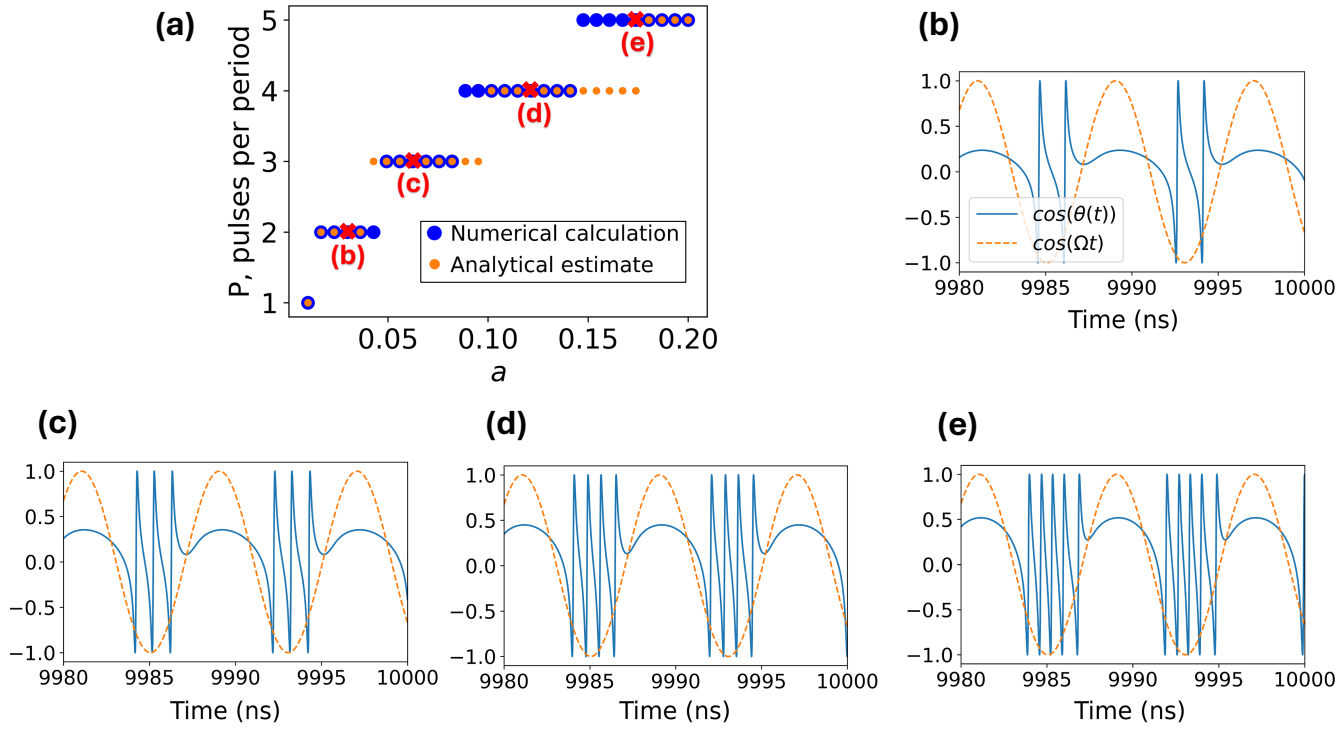

Figure 7: Multi-pulse generation in the phenomenological model. (a) Number of pulses per period as a function of the modulation amplitude a, computed from direct numerical simulations of the phenomenological model (4) (blue dots) and from the analytical prediction based on Eqs. (13)-(14), with only the integer part p shown (orange dots). (b)-(e) Time traces $\theta(t)$ (blue) and $\cos(\Omega t)$ (orange) for representative cases with increasing numbers of pulses per period: (b) two pulses per period, $a = 0.03$, (c) three pulses per period, $a = 0.07$, (d) four pulses per period, $a = 0.12$, (e) five pulses per period, $a = 0.017$. $\Omega = 0.785$ corresponds to the time period of η in the reduced model in Fig. 6(a). $\kappa^f = 17.52$ ns^{-1}.

where the integral in the denominator can be calculated symbolically as:

$$\int \frac{2\pi}{\sqrt{\nu^2-(1+a\cos(\psi))^2}}d\psi = \frac{32\pi\cos^2\left(\frac{\psi}{2}\right)\sqrt{\frac{a\cos(\psi)-\nu+1}{(a-\nu+1)(\cos(\psi)+1)}}\sqrt{\frac{a\cos(\psi)+\nu+1}{(a+\nu+1)(\cos(\psi)+1)}}\sqrt{\frac{-a^2\cos^2(\psi)-2a\cos(\psi)+\nu^2-1}{(\cos(\psi)+1)^2}}\mathcal{F}}{\sqrt{\frac{a-\nu-1}{a+\nu+1}}\sqrt{a^2(-\cos(2\psi))-a^2-4a\cos(\psi)+2\nu^2-2}\sqrt{-\sec^4\left(\frac{\psi}{2}\right)\left(a^2\cos(2\psi)+a^2+4a\cos(\psi)-2\nu^2+2\right)}}, \tag{14}$$

with $\mathcal{F} = F\left(\sin^{-1}\left(\sqrt{\frac{a-\nu-1}{a+\nu+1}}\tan\left(\frac{\psi}{2}\right)\right)\middle|\frac{(a+\nu-1)(a+\nu+1)}{a^2-2\nu a+\nu^2-1}\right)$, where $F(x|m)$ is the elliptic integral of the first kind. By rescaling the parameters in (13)-(14) back to the original parameters in the phenomenological model (4) and taking the integer part to ensure $p \in \mathbb{Z}$, we arrive at the general formula (5) for predicting the number of pulses per cycle. This formula is used to generate the analytical estimate shown in Fig. 7(a).

Supporting Information

Supporting Information is available from the Wiley Online Library or from the author.

Acknowledgements

This work is supported by the Office of Naval Research. The authors thank Vladimir Belykh for his invaluable input, Mark A. Berrill for his help in developing optimized numerical tools for the time-delayed system simulations, and Matthew Crespo for his initial work on the topic of pulsing laser arrays.

References

[1] P. R. Prucnal, B. J. Shastri, T. Ferreira de Lima, M. A. Nahmias, A. N. Tait, *Advances in Optics and Photonics* **2016**, *8*, 2 228.

[2] J. Robertson, E. Wade, Y. Kopp, J. Bueno, A. Hurtado, *IEEE Journal of Selected Topics in Quantum Electronics* **2020**, *26*, 1 7700715.

[3] M. Nakajima, K. Tanaka, T. Hashimoto, *Communications Physics* **2021**, *4*, 1 20.

[4] M. Zbik, In *CLEO: Applications and Technology*. Optica Publishing Group, **2019** AF3K–7.

[5] Y. Chen, H. Winful, J. Liu, *Applied Physics Letters* **1985**, *47*, 3 208.

[6] E. Hemery, L. Chusseau, J.-M. Lourtioz, *IEEE Journal of Quantum Electronics* **1990**, *26*, 4 633.

[7] J. R. Tredicce, F. T. Arecchi, G. L. Lippi, G. P. Puccioni, *JOSA B* **1985**, *2*, 1 173.

[8] S. Wieczorek, B. Krauskopf, D. Lenstra, *Physical Review Letters* **2002**, *88*, 6 063901.

[9] D. Goulding, S. P. Hegarty, O. Rasskazov, S. Melnik, M. Hartnett, G. Greene, J. G. McInerney, D. Rachinskii, G. Huyet, *Physical Review Letters* **2007**, *98*, 15 153903.

[10] P. Downey, J. Bowers, R. Tucker, E. Agyekum, *IEEE Journal of Quantum Electronics* **1987**, *23*, 6 1039.

[11] H.-F. Liu, M. Fukazawa, Y. Kawai, T. Kamiya, *IEEE Journal of Quantum Electronics* **1989**, *25*, 6 1417.

[12] H. Haus, *IEEE Journal of Quantum Electronics* **1975**, *11*, 7 323.

[13] X. Liu, Y. Cui, *Advanced Photonics* **2019**, *1*, 1 016003.

[14] H. A. Haus, *Journal of Applied Physics* **1975**, *46*, 7 3049.

[15] D. Puzyrev, A. Vladimirov, A. Pimenov, S. Gurevich, S. Yanchuk, *Physical Review Letters* **2017**, *119*, 16 163901.

[16] A. Perego, M. Lamperti, *Physical Review A* **2016**, *94*, 3 033839.

[17] K. Alfaro-Bittner, S. Barbay, M. Clerc, *Chaos: An Interdisciplinary Journal of Nonlinear Science* **2020**, *30*, 8 083136.

[18] O. Spitz, L. E. Maldonado-Castillo, M. A. Berrill, Y. Braiman, *IEEE Journal of Selected Topics in Quantum Electronics* **2025**, *31*, 2 1501614.

[19] M. Münkel, F. Kaiser, O. Hess, *International Journal of Bifurcation and Chaos* **1998**, *8*, 05 951.

[20] A. Scirè, C. J. Tessone, P. Colet, *IEEE Journal of Quantum Electronics* **2005**, *41*, 3 272.

[21] M. Münkel, F. Kaiser, O. Hess, *Physical Review E* **1997**, *56*, 4 3868.

[22] K. Otsuka, J.-L. Chern, *Physical Review A* **1992**, *45*, 7 5052.

[23] H. G. Winful, L. Rahman, *Physical Review Letters* **1990**, *65*, 13 1575.

[24] T. Sugawara, M. Tachikawa, T. Tsukamoto, T. Shimizu, *Physical Review Letters* **1994**, *72*, 22 3502.

[25] R. Roy, K. S. Thornburg Jr, *Physical Review Letters* **1994**, *72*, 13 2009.

[26] G. Kozyreff, A. Vladimirov, P. Mandel, *Physical Review E* **2001**, *64*, 1 016613.

[27] C. Masoller, *Physical Review Letters* **2001**, *86*, 13 2782.

[28] Y. C. Kouomou, P. Colet, N. Gastaud, L. Larger, *Physical Review E* **2004**, *69*, 5 056226.

[29] J. Zamora-Munt, C. Masoller, J. Garcia-Ojalvo, R. Roy, *Physical Review Letters* **2010**, *105*, 26 264101.

[30] M. Nixon, M. Fridman, E. Ronen, A. A. Friesem, N. Davidson, I. Kanter, *Physical Review Letters* **2012**, *108*, 21 214101.

[31] F. Grillot, A. Gavrielides, O. Spitz, T. C. Newell, M. Carras, In *Quantum Sensing and Nano Electronics and Photonics XV*, volume 10540. SPIE, **2018** 224–231.

[32] J. Ding, I. Belykh, A. Marandi, M.-A. Miri, *Physical Review Applied* **2019**, *12*, 5 054039.

[33] M. Honari-Latifpour, J. Ding, I. Belykh, M.-A. Miri, *Chaos: An Interdisciplinary Journal of Nonlinear Science* **2025**, *35*, 2 021101.

[34] J. Sheng, X. Wei, C. Yang, H. Wu, *Physical Review Letters* **2020**, *124*, 5 053604.

[35] J. Hillbrand, D. Auth, M. Piccardo, N. Opačak, E. Gornik, G. Strasser, F. Capasso, S. Breuer, B. Schwarz, *Physical Review Letters* **2020**, *124*, 2 023901.

[36] M. Khajavikhan, A. Hoyer-Leitzel, J. R. Leger, *Optics Letters* **2008**, *33*, 20 2377.

[37] P. Nyaupane, O. Spitz, G. Scranton, S. Koyu, M. A. Berrill, P. L. LiKamWa, Y. Braiman, *ACS Photonics* **2025**, *12*, 2 597.

[38] Y. Braiman, J. F. Lindner, W. L. Ditto, *Nature* **1995**, *378*, 6556 465.

[39] Y. Braiman, W. Ditto, K. Wiesenfeld, M. Spano, *Physics Letters A* **1995**, *206*, 1-2 54.

[40] T. Nishikawa, A. E. Motter, *Physical Review Letters* **2016**, *117*, 11 114101.

[41] I. Belykh, R. Jeter, V. Belykh, *Science Advances* **2017**, *3*, 11 e1701512.

[42] J. D. Hart, Y. Zhang, R. Roy, A. E. Motter, *Physical Review Letters* **2019**, *122*, 5 058301.

[43] K. Daley, K. Zhao, I. V. Belykh, *Chaos: An Interdisciplinary Journal of Nonlinear Science* **2020**, *30*, 4 043102.

[44] Y. Zhang, J. L. Ocampo-Espindola, I. Z. Kiss, A. E. Motter, *Proceedings of the National Academy of Sciences* **2021**, *118*, 21 e2024299118.

[45] F. Molnar, T. Nishikawa, A. E. Motter, *Nature Communications* **2021**, *12*, 1 1457.

[46] N. Punetha, L. Wetzel, *Physical Review E* **2022**, *106*, 5 L052201.

[47] Y. Eliezer, S. Mahler, A. A. Friesem, H. Cao, N. Davidson, *Physical Review Letters* **2022**, *128*, 14 143901.

[48] B. Liu, Y. Liu, Y. Braiman, *Optics Express* **2008**, *16*, 25 20935.

[49] B. Liu, Y. Braiman, *Optics Express* **2013**, *21*, 25 31218.

[50] N. Nair, K. Hu, M. Berrill, K. Wiesenfeld, Y. Braiman, *Physical Review Letters* **2021**, *127*, 17 173901.

[51] S. Yanchuk, S. Ruschel, J. Sieber, M. Wolfrum, *Physical Review Letters* **2019**, *123*, 5 053901.

[52] L. Munsberg, J. Javaloyes, S. V. Gurevich, *Chaos: An Interdisciplinary Journal of Nonlinear Science* **2020**, *30*, 6 063137.

[53] B. Garbin, J. Javaloyes, G. Tissoni, S. Barland, *Nature Communications* **2015**, *6*, 1 5915.

[54] S. H. Strogatz, *Nonlinear dynamics and chaos: with applications to physics, biology, chemistry, and engineering*, CRC press, **2018**.

[55] Z. Chen, M. Segev, D. N. Christodoulides, *Reports on Progress in Physics* **2012**, *75*, 8 086401.

[56] R. Lang, K. Kobayashi, *IEEE Journal of Quantum Electronics* **1980**, *16*, 3 347.

[57] T. Heil, I. Fischer, W. Elsäßer, B. Krauskopf, K. Green, A. Gavrielides, *Physical Review E* **2003**, *67*, 6 066214.

[58] A. Tabaka, K. Panajotov, I. Veretennicoff, M. Sciamanna, *Physical Review E* **2004**, *70*, 3 036211.

[59] C. Masoller, *Chaos: An Interdisciplinary Journal of Nonlinear Science* **1997**, *7*, 3 455.

[60] J.-X. Dong, J. Ruan, L. Zhang, J.-P. Zhuang, S.-C. Chan, *Physical Review A* **2021**, *103*, 5 053524.

[61] D. Baums, W. Elsässer, E. O. Göbel, *Physical Review Letters* **1989**, *63*, 2 155.

[62] X. Wu, Y. Zhang, J. Peng, S. Boscolo, C. Finot, H. Zeng, *Nature Communications* **2022**, *13*, 1 5784.

[63] G. Liu, X. Ma, K. Zhou, B. Liu, L. Zheng, X. Bi, S. Wu, Y. Lu, Z. Li, W. Wan, Z. Zhang, J. Peng, Y. Zhang, H. Zeng, H. Li, *Light: Science & Applications* **2025**, *14*, 1 147.

[64] J. A. Acebrón, L. L. Bonilla, C. J. Pérez Vicente, F. Ritort, R. Spigler, *Reviews of Modern Physics* **2005**, *77*, 1 137.

[65] D. Kazakov, N. Opačak, F. Pilat, Y. Wang, A. Belyanin, B. Schwarz, F. Capasso, *APL Photonics* **2024**, *9*, 2 026104.

[66] I. Joindot, *Journal de Physique III* **1992**, *2*, 9 1591.

[67] H. Kim, P. Didier, S. Zaminga, D. A. Díaz-Thomas, A. Baranov, J.-B. Rodriguez, E. Tournié, H. Knötig, B. Schwarz, L. Cerutti, et al., *APL Photonics* **2024**, *9*, 10.

[68] Z. Wu, S. You, Q. Du, Y. Huang, *Optics Communications* **2020**, *471* 126031.

[69] P. Gandhi, E. Knobloch, C. Beaume, *Physical Review E* **2015**, *92*, 6 062914.

[70] P. W. Smith, M. Duguay, E. Ippen, *Progress in Quantum Electronics* **1974**, *3* 107.

[71] D. Kazakov, T. P. Letsou, M. Piccardo, L. L. Columbo, M. Brambilla, F. Prati, S. Dal Cin, M. Beiser, N. Opačak, P. Ratra, et al., *Nature* **2025**, *641* 83.

[72] P. Genevet, S. Barland, M. Giudici, J. R. Tredicce, *Physical Review A* **2009**, *79*, 3 033819.

Gregg Scranton received his Ph.D. from the University of California, Berkeley in 2017. His research focused on EUV lithography and thermo-photovoltaics. He worked at ASML for 3.5 years, applying machine learning to lithographic mask design. He is now a postdoctoral researcher at the University of Central Florida, focused on computational optics and nonlinear systems.

Kendall Golden received his B.S. degree in Mathematics from the University of Alabama in 2021. He is currently pursuing a Ph.D. degree in Mathematics and Statistics at Georgia State University. His research interests include dynamical systems and synchronization with applications to lasers and neuroscience.

Olivier Spitz received his Ph.D. in electrical engineering from Université Paris-Saclay, Saclay, France, in 2019, under the supervision of Prof. Frédéric Grillot. He was awarded the Springer-Nature outstanding thesis prize as well as the Délégation Générale de l'Armement (DGA) thesis prize for his work on the nonlinear dynamics of quantum cascade lasers under external optical feedback/injection. He is now a postdoctoral researcher at the University of Central Florida, Orlando, FL. Dr. Spitz is a member of SPIE, the IEEE Photonics Society, the American Vacuum Society, and Optica.

Arindam Mishra received his Ph.D. from Jadavpur University, Kolkata, India, in 2019. He is currently a Postdoctoral Scholar at CREOL – The College of Optics and Photonics at the University of Central Florida. Prior to this, he was a Research Fellow at the National University of Singapore. His research interests lie broadly in nonlinear dynamics, chaos, and complex networks. At present, his work focuses on modeling the dynamics of semiconductor lasers.

Igor Belykh received the Ph.D. degree in Applied Mathematics from the University of Nizhny Novgorod, Russia, in 2000. From 2001 to 2005, he was a postdoctoral fellow in the Laboratory of Nonlinear Systems at École Polytechnique Fédérale de Lausanne (EPFL), Switzerland. Since 2006, he has been with Georgia State University, where he holds the position of Distinguished University Professor of Applied Mathematics with a joint appointment in the Neuroscience Institute. His research interests include nonlinear dynamics, synchronization phenomena, and complex networks with applications in laser systems, neuroscience, and engineering. Dr. Belykh is a Senior Member of IEEE and a member of SIAM.

Yehuda Braiman received the Ph.D. degree from the University of Tel Aviv in 1993. Since 2020, he has been a Research Professor at the College of Optics and Photonics, Center for Research and Education in Optics and Lasers (CREOL), University of Central Florida. Prior to that, he was a Distinguished Research Staff Member at the Oak Ridge National Laboratory and a Joint Faculty Professor in the Department of Mechanical, Aerospace, and Biomedical Engineering at the University of Tennessee. His current research interests include synchronization and coherent beam combining of high-power arrays of semiconductor and fiber lasers, and nonlinear dynamics and disorder-promoted synchronization in coupled semiconductor diode lasers and nonlinear oscillator arrays. Dr. Braiman is a member of the American Physical Society and a Senior member of Optica.

Table of Contents

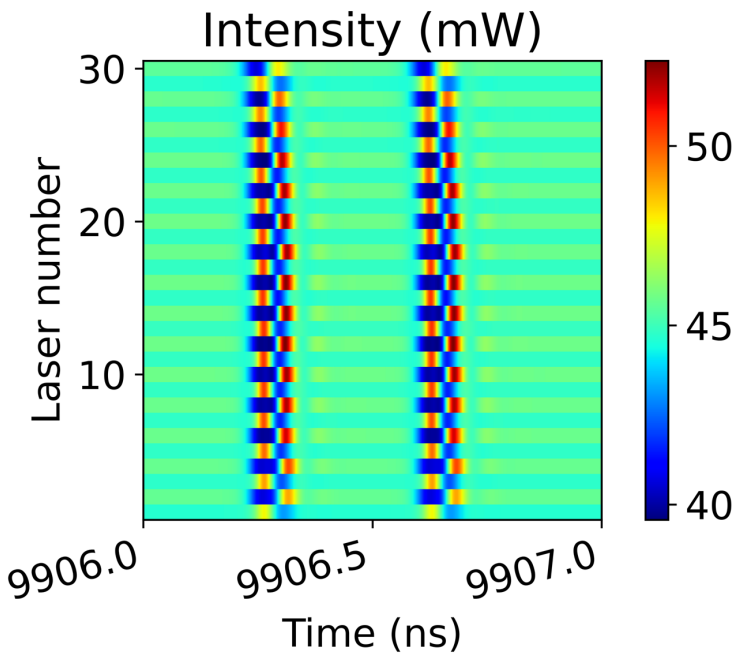

Controllable pulsing in an array of semiconductor lasers with engineered heterogeneity